POLITECNICO DI TORINO
Repository ISTITUZIONALE

Parametric modeling of cradle-to-gate carbon emissions from gas-atomized AISI 316L powders under closed-loop feedstock strategies

Original
Parametric modeling of cradle-to-gate carbon emissions from gas-atomized AISI 316L powders under closed-loop feedstock strategies / Priarone, P.C., Gobber, F.S., Cacace, S.. - In: POWDER TECHNOLOGY. - ISSN 0032-5910. - STAMPA. - 470:(2026), pp. 1-12. [10.1016/j.powtec.2025.121949]

Availability:
This version is available at: 11583/3008505 since: 2026-03-10T11:30:56Z

Publisher:
Elsevier B.V.

Published
DOI:10.1016/j.powtec.2025.121949

Terms of use:

This article is made available under terms and conditions as specified in the corresponding bibliographic description in the repository

Publisher copyright

(Article begins on next page)

27 November 2026

Powder Technology 470 (2026) 121949

Contents lists available at ScienceDirect

Powder Technology

journal homepage: www.journals.elsevier.com/powder-technology

Parametric modeling of cradle-to-gate carbon emissions from gas-atomized AISI 316L powders under closed-loop feedstock strategies

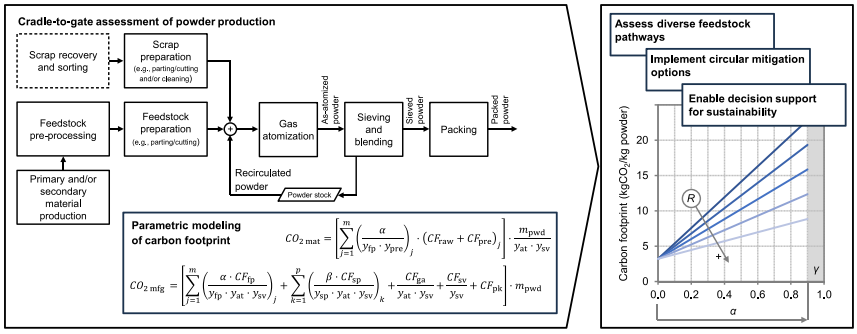
Paolo C. Priarone [a,*], Federico Simone Gobber [b], Stefania Cacace [c]

[a] Politecnico di Torino, Department of Management and Production Engineering, Corso Duca degli Abruzzi 24, 10129 Torino, Italy
[b] Politecnico di Torino, Department of Applied Science and Technology, Viale Teresa Michel 5, 15121 Alessandria, Italy
[c] Politecnico di Milano, Department of Mechanical Engineering, Via La Masa 1, 20156 Milano, Italy

HIGHLIGHTS

- A parametric model quantifies cradle-to-gate CO_2 emissions of AISI 316L powders.
- Multiple feedstock configurations are analyzed for gas atomization.
- Primary raw material sourcing could significantly affect CO_2 emissions.
- Closed-loop strategies could contribute to lowering the environmental footprint.
- The framework suggests decarbonization paths for sustainable powder production.

GRAPHICAL ABSTRACT



ARTICLE INFO

Keywords:
Sustainable manufacturing
Carbon footprint
Metal powder production
Waste recycling
Closed-loop material modeling

ABSTRACT

This study introduces a parametric framework for the cradle-to-gate assessment of carbon emissions associated with the production of gas-atomized AISI 316L stainless steel powders intended for use in additive manufacturing and other powder metallurgy processes. The model provides a detailed representation of upstream material flows and includes all major unit operations involved in powder production, such as feedstock preparation, gas atomization, sieving and blending, and packing. By varying the composition of the feedstock charged into the atomizer crucible, the framework enables the estimation of carbon emissions across a wide range of scenarios reflecting alternative sourcing strategies. The case study on AISI 316L highlights the environmental benefits of integrating closed-loop material flows, including the recirculation of off-specification powders and the direct use of compatible metallic scrap. Furthermore, broadening the acceptable powder size range significantly improves atomization yield, thereby reducing the specific carbon intensity of usable powder output. Such an approach lays the foundation for the development of robust decision-support tools for process planning in gas atomization, with direct implications for industrial-scale powder production.

* Corresponding author.
E-mail address: paoloclaudio.priarone@polito.it (P.C. Priarone).

https://doi.org/10.1016/j.powtec.2025.121949
Received 1 September 2025; Received in revised form 9 November 2025; Accepted 19 November 2025
Available online 22 November 2025
0032-5910/© 2025 The Authors. Published by Elsevier B.V. This is an open access article under the CC BY-NC-ND license (http://creativecommons.org/licenses/by-nc-nd/4.0/).

1. Introduction

Industry and manufacturing significantly contribute to global environmental impacts. According to the International Energy Agency [1], energy accounts for more than three-quarters of total greenhouse gas (GHG) emissions globally, and industry contributed to nearly 38 % of global fuel combustion emissions in 2022. This is particularly evident in energy- and resource-intensive sectors [2,3]. As industries strive to meet increasingly stringent climate targets and sustainability goals, attention has shifted toward alternative production technologies that offer improved resource efficiency and lower environmental footprints.

Additive Manufacturing (AM) has emerged as a promising enabler of more sustainable industrial practices, owing to its inherent capabilities such as near-net-shape fabrication, design freedom, on-demand production, increased material usage efficiency, and the elimination of dedicated tooling [4,5]. These features allow for significant reductions in material waste, enhanced part performance through topological optimization and part consolidation, and potential improvements in logistics through localized and digitalized production models. For these reasons, AM is being increasingly adopted in high-impact sectors such as aerospace [6], automotive [7,8], and oil & gas [9], where complex, high-value components can benefit from the process unique advantages. Among metal AM technologies, laser powder bed fusion (PBF-LB/M) stands out for its ability to manufacture dense, high-performance parts with intricate geometries. However, despite its downstream benefits, recent life cycle assessments (LCAs) have highlighted critical sustainability trade-offs in powder-based AM [10]. Powder manufacturing, especially via gas atomization, is both energy- and resource-intensive. Life-cycle assessments report global warming potentials of 0.7–24.8 kg CO_2-eq per kg of powder and cumulative energy demands of 37–602 MJ per kg, depending on the atomization method [4]. As highlighted in recent reviews, the atomization stage can contribute up to ≈55 % of the total GWP in the life cycle of metal additive manufacturing [11]. These impacts can offset the downstream sustainability benefits of AM, raising critical questions about the overall environmental balance of powder-based AM workflows [12].

In many cases, the environmental burden of powder production exceeds that of the AM process itself. At the industrial scale, metal powders are produced via melt-based, solid-state, or chemical routes. Among the melt-based techniques, water atomization (WA) and gas atomization (GA) account for the largest share, with variants including close-coupled or free-fall designs, as well as crucible-free electrode induction melting gas atomization (EIGA), plasma atomization (PA), and centrifugal methods such as the plasma rotating electrode process (PREP). Solid-state/chemical routes encompass hydride–dehydride (HDH), carbonyl, and mechanical milling [13]. These routes involve well-known trade-offs in particle morphology and surface condition, oxygen/nitrogen pickup, particle size distribution (PSD), throughput, and cost. For applications requiring spherical and thus highly flowable powders with low contamination, typical of metal AM workflows, melt atomization is predominantly employed across the supply chain [14]. Within melt atomization, inert gas atomization remains the most widely adopted technique for producing spherical, high-quality feedstocks across a broad alloy palette (Al, steels, Ni/Co superalloys), as it combines near-spherical morphology, reduced oxygen uptake, and tight PSD control with industrial throughput and cost competitiveness relative to PA, PREP, and EIGA. By contrast, WA is highly productive and cost-effective but generally yields more irregular and more oxidized particles (2000–5000 ppm [15]), which may penalize flowability and apparent density in demanding PBF-LB/M processes unless additional conditioning is applied [16]. Premium processes such as PA, PREP, and EIGA deliver clean and highly spherical powders (especially for reactive alloys such as Ti-6Al-4V) but usually at higher cost and, in some cases, with feedstock-form constraints (wire or electrode) [17]. They are therefore reserved for applications where a higher grade of cleanliness and sphericity is required.

The production of metal powders suitable for PBF-LB/M via gas atomization requires high-temperature melting, the use of inert or reactive gases, and multiple post-processing steps including sieving and classification. Moreover, typical yields from gas atomization can be low, with only a fraction of the atomized material meeting the particle size and morphology specifications for PBF-LB/M, further amplifying resource consumption [18]. Given this context, decarbonizing the metal powder supply chain is essential to improving the sustainability profile of AM. Two main strategies have been proposed to mitigate the environmental impact of metal powders in AM: (*i*) reducing powder consumption through process optimization and powder reuse, and (*ii*) lowering the impact of powder production by incorporating secondary raw materials. The former includes measures such as optimizing build orientation or reusing powders recovered and sieved after previous additive manufacturing build cycles. The latter involves sourcing feedstock from pre-consumer scrap or other waste streams. In contrast to residual powder reuse, which generally requires only re-screening, the recycling of secondary metallic feedstock necessitates complete re-melting and atomization to produce powders that meet the stringent quality requirements of AM applications.

1.1. Use of secondary feedstock in powder production

In response to growing sustainability concerns in additive manufacturing, a number of studies have investigated the use of recycled and secondary materials as feedstock for powder production, particularly for PBF-LB/M applications. A key challenge in this context lies in assuring the in-use performance of the final parts, given that powder characteristics such as particle morphology, size distribution, flowability, and chemical composition critically influence process stability and mechanical integrity. Various routes for converting metallic scrap, and especially titanium alloys, into AM-grade powder have been explored. For instance, Dhiman et al. [19] proposed a general framework for recycling machining chips into spherical powders using advanced mechanical processing, emphasizing the trade-offs in terms of energy, morphology, and powder consistency. Building on this, Dhiman et al. [20] demonstrated that multi-stage ball milling of Ti-6Al-4V swarf can yield powders with size and shape characteristics comparable to those obtained by gas atomization, suitable for direct metal laser sintering. Similarly, Gökelma et al. [21] successfully employed the hydrogenation–dehydrogenation method on Ti-6Al-4V machining turnings, producing powders that met flow and purity requirements for cold spray and potentially AM processes.

Beyond laboratory-scale mechanical recycling, several efforts have addressed the feasibility of using recycled metal charge in gas atomization, which is the most common industrial method for AM powder production. Cacace et al. [22], Tebaldo et al. [23] and Gobber et al. [24] investigated the use of secondary materials in the gas atomization of AISI 316L, titanium alloys and UNS S32760 super duplex steel, respectively. These studies report that, while feasible, the use of recycled feedstock can influence yield, oxygen content, and particle morphology, thus requiring tight control of processing parameters and post-atomization screening to ensure powder suitability. In a comparative life cycle assessment, Benedetti et al. [25] showed that the environmental benefits of using recycled charge in powder production are significant, particularly when integrated into closed-loop AM workflows. Crucially, their work also included mechanical and fatigue testing of PBF-LB/M specimens, showing no significant difference in fatigue life between parts made from virgin and recycled powder, under equivalent processing conditions. From a performance standpoint, Richter et al. [26] provided additional validation by demonstrating that Ti-6Al-4V parts manufactured via electron beam powder bed fusion from mechanically recycled powder – obtained through comminution of support structures – exhibited mechanical and fatigue behavior comparable to parts built from virgin powders. Singh et al. [27] further contributed to this line of evidence by conducting a systematic comparison between

powders produced from virgin and recycled Ti-6Al-4V feedstock. Their analysis included morphology, chemistry, and flowability of the powders, as well as mechanical testing of samples produced via laser powder bed fusion. While overall results confirmed the technical viability of using recycled input material, the study highlighted that minor differences in oxygen content and particle morphology could influence laser–material interaction and melt pool dynamics.

1.2. Literature gap and aim of the study

Overall, the limited body of literature referenced in Section 1.1 has demonstrated the technical feasibility of producing powders from predominantly homogeneous scrap or single-alloy recycled materials. These studies frequently report powder characteristics comparable to those obtained from virgin feedstocks. It is worth noting that remelting scrap in a vacuum induction melting (VIM) furnace, combined with careful selection of crucible materials and an inert atmosphere, can effectively reduce oxygen and nitrogen levels, even for nickel-based superalloy scraps, where strict control of chemical composition is required [28]. For AISI 316L, remelting waste or scrap through a VIM-based route can yield AM-grade powder with low oxygen content (~234 ppm) and, consequently, excellent processability [29].

Where environmental assessments have been conducted, such approaches have shown notable reductions in carbon emissions, particularly when applying the recycled content allocation method, which attributes minimal upstream environmental impact to recycled and/or secondary inputs. However, few studies have addressed more complex feedstock scenarios involving mixed streams, nor have they systematically quantified the environmental trade-offs associated with varying input compositions. Additionally, although the influence of recycled inputs on powder quality and downstream part performance is acknowledged, the literature lacks systematic criteria for evaluating the environmental effects in a consistent manner.

This study aims to partially address this knowledge gap by developing a parametric model to quantify the carbon emissions associated with the production of gas-atomized AISI 316L powder, with a particular focus on applications in PBF-LB/M. The model encompasses the major unit processes and supports the analysis of a broad range of feedstock compositions, including mixtures of primary materials, off-specification powders, and metallic scrap, with an emphasis on the integration of closed-loop material flows. The model is introduced in Section 2 and applied to selected case studies of industrial relevance in Section 3. Results are discussed in Section 4, and conclusions along with perspectives for future research are provided in Section 5.

2. Materials and methods

The objective of this study is to develop a modeling framework aimed at quantifying and comparing the carbon footprint of gas-atomized powders produced with varying proportions of heterogeneous input materials fed into the atomizer – including bulky scrap, metal feedstocks with different recycled content levels, and recirculated powders from previous atomization processes – each characterized by a distinct environmental profile. A life cycle perspective is adopted in accordance with ISO 14040/44 standards [30,31] and the guidelines set forth in the ILCD Handbook [32]. The functional unit for the analysis is defined as one unit of mass (1 kg) of powder produced in a usable size range, with varying shares of input sources. The system boundaries for the carbon footprint assessment are set to a cradle-to-gate scope (as shown in Fig. 1), encompassing both raw material production and powder manufacturing stages [33]. The recycled content allocation approach is consistently applied [34]. Primary data were collected from an industrial powder manufacturer and supplemented with secondary data from Granta Selector 2025 for upstream processes. The impact of transporting the materials – either from material suppliers or waste collectors to the powder production plant, and subsequently to the end user – was found to be negligible on a per-kilogram basis (accounting for less than 1 % of the total carbon footprint), assuming European road transport distances and a standard emission factor for a 32-ton truck of 0.072 $kgCO_2$/ton·km [35].

2.1. Material flows

The mass of material charged into the atomizer crucible (m_{ch}) is related to the mass of powder packed and prepared for shipment (m_{pwd}) according to Eq.1,

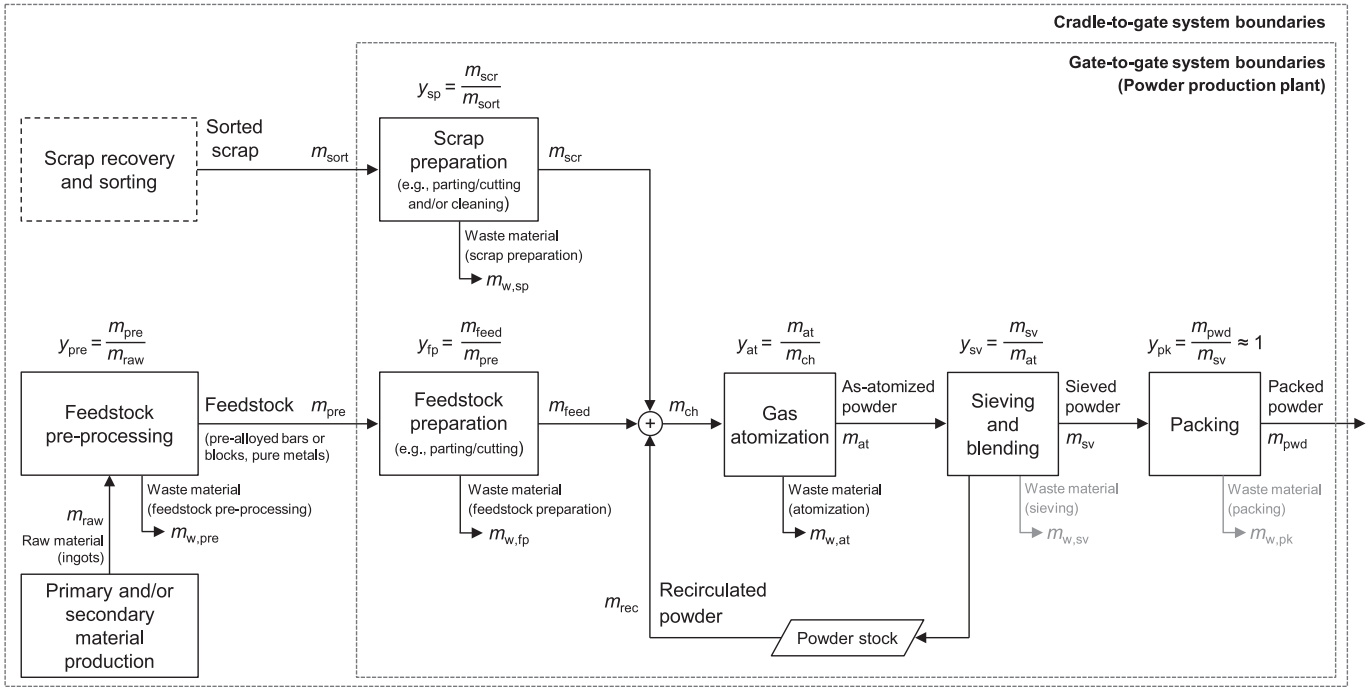


Fig. 1. System boundaries for powder carbon footprint assessment, highlighting the material flows.

$$m_{ch} = \frac{m_{pwd}}{\prod_{i=1}^{n} y_i} \tag{1}$$

where the denominator represents the product of the i-th yield factors (y_i) for each of the n unit processes involved in powder production. Each yield factor corresponds to the fraction of material retained through a specific process, including (*i*) gas atomization, (*ii*) sieving and blending, and (*iii*) packing. As such, all potential material loss streams are taken into consideration. The atomization yield (y_{at}), defined as the ratio of the mass of powder collected in atomizer, regardless of size (m_{at}), to the mass of material loaded into the crucible (m_{ch}), reflects losses occurring during the atomization process ($m_{w,at}$) due to vaporized material, fine dust trapped within the atomizer chamber and filters, and slag adhered to the crucible. For the sieving and blending operations, the yield factor (y_{sv}) defines the proportion of usable powder (m_{sv}) – with granulometry within the range specified for the industrial application (e.g., 20–63 μm for PBF-LB/M) – relative to the total atomized powder mass (m_{at}). During sieving, over- and under-sized particles are discarded and may be recirculated back as feedstock material for subsequent atomization cycles. In such cases, recirculated powder is not considered waste, but rather a closed-loop material flow. Unrecoverable material waste in sieving and blending ($m_{w,sv}$) are therefore limited to the powder that cannot be recovered, such as ultra-fine particles lost during equipment cleaning, which are expected to be negligible, as is the amount of powder lost ($m_{w,pk}$) during the packing process into plastic containers for shipment (i.e., the packing yield, $y_{pk} = 1$). Based on these considerations, the mass of material required for atomization is quantified in this study according to Eq. 2.

$$m_{ch} = \frac{m_{pwd}}{y_{at} \cdot y_{sv}} \tag{2}$$

The gas atomization process can receive a variety of material inputs, as illustrated in Fig. 1, including: (*i*) metal feedstock derived from primary and/or secondary material production (m_{feed}), such as bars, blocks or castings made of pre-alloyed material or pure metals; (*ii*) powders that are recirculated (m_{rec}) from previous atomization cycles; and (*iii*) bulky scraps (m_{scr}), which may be recovered from end-of-life components or manufacturing waste. As a result, focusing on the upstream material flow, the mass of material charged into the atomizer crucible (m_{ch}) can be written according to Eq. 3,

$$m_{ch} = m_{feed} + m_{scr} + m_{rec} = (\alpha + \beta + \gamma) \cdot m_{ch} \tag{3}$$

where $\alpha = \frac{m_{feed}}{m_{ch}}; \beta = \frac{m_{scr}}{m_{ch}}; \gamma = \frac{m_{rec}}{m_{ch}}$

In principle, under these definitions, each of the three normalized mass input flows (α, β, and γ) can assume values in the range [0,1]. However, technological and quality constraints impose additional limitations on their feasible domains. Based on industrial practice and alloy-specific considerations, approximate bounds on the normalized inputs are defined in this study, as detailed in the data inventory presented in the following Section 3. Furthermore, as both m_{feed} and m_{scr} may originate from m-th and p-th heterogeneous input streams – such as pre-alloyed materials and pure metals, each characterized by distinct carbon footprints, or diverse bulky scrap sources – Eq. 3 can be generalized as Eq. 4.

$$m_{ch} = \sum_{j=1}^{m} (m_{feed})_j + \sum_{k=1}^{p} (m_{scr})_k + m_{rec} \tag{4}$$

To quantify the total material input (m_{mat}) required to produce a unit mass of powder (m_{pwd}), the material losses incurred during charge preparation should be taken into account. These losses may arise from cutting operations performed to adapt feedstock materials (with mass m_{pre}) to the crucible geometry, generating waste $m_{w,fp}$, and, in the case of recovered and sorted scrap materials (with mass m_{sort}), from the removal of surface layers that may be oxidized or contaminated, resulting in waste $m_{w,sp}$. When the incoming feedstock portfolio is appropriately selected, the magnitude of these losses is generally limited. Nonetheless, charge preparation operations – such as bar cutting or surface milling of bulky scrap – can generate waste amounting to a few percent of the input weight, depending on the geometry and the specific scrap conditions. Therefore, two distinct yield factors (y_{fp} and y_{sp}) have been introduced in the model.

In addition, referring to Fig. 1, when the metal feedstock originates from primary and/or secondary material production, the calculation of required raw material (m_{raw}) has to incorporate the material losses ($m_{w,pre}$) associated with pre-manufacturing processes that transform raw materials – typically in the form of ingots – into commercially-available semi-manufactured components such as blocks or bars. Given the yield factors of these unit processes (y_{pre}), m_{mat} is determined according to Eq. 5,

$$\begin{aligned} m_{mat} &= \sum_{j=1}^{m} \left(\frac{m_{feed}}{y_{fp} \cdot y_{pre}} \right)_j + \sum_{k=1}^{p} \left(\frac{m_{scr}}{y_{sp}} \right)_k + m_{rec} \\ &= \left[\sum_{j=1}^{m} \left(\frac{\alpha}{y_{fp} \cdot y_{pre}} \right)_j + \sum_{k=1}^{p} \left(\frac{\beta}{y_{sp}} \right)_k + \gamma \right] \cdot \frac{m_{pwd}}{y_{at} \cdot y_{sv}} \end{aligned} \tag{5}$$

where the recirculated powder is assumed to be directly reusable as atomization feedstock without undergoing further processing losses.

2.2. Carbon footprint of input materials

The practice of recycling gives rise to allocation issues, as the environmental impacts associated with the unit processes involved in the extraction and processing of raw materials, as well as the final disposal of products (including recycling), are shared by the product systems that deliver and receive the recycled material [33]. In accordance with the system boundaries, the recycled content (100:0) approach is applied, whereby the sole environmental burden associated with secondary raw materials is that pertaining to the process utilized for their recycling. Therefore, for all feedstocks involving primary or secondary material production, or a combination thereof, the effective embodied impacts are calculated according to Eq. 6,

$$CF_{raw} = (1 - R) \cdot CF_V + R \cdot CF_R = CF_V - R \cdot (CF_V - CF_R) \tag{6}$$

where:

- CF_{raw} is the effective embodied impact per unit mass of material (e.g., the carbon footprint, in $kgCO_2/kg$);
- CF_V is the embodied impact arising from virgin material input (primary production) per unit mass of material;
- CF_R is the embodied impact arising from recycled material input (secondary production) per unit mass of material;
- R is the recycled content.

Eq. 6 can be derived from Ref. [34] on the assumption that the impact of waste disposal is negligible per unit mass of material. This is consistent with the first-order energy and carbon penalties of 0.1 MJ and 0.01 $kgCO_2$ per kg of disposed material, as suggested by Ashby [35]. Additionally, the same equation can be retrieved by applying the Circular Footprint Formula for PEF assessment (Ref. [36], Section 4.4.8.1) to cradle-to-gate studies (Ref. [36], Section 4.4.8.12) with the value of the A parameter set to 1. Eq. 6 implies that the benefits of material recycling are contingent upon the displacement of virgin (primary) materials by secondary materials. As the recycled content increases, the effective embodied impact decreases; for $R = 1$ (i.e., 100 %-recycled materials), CF_{raw} is equivalent to CF_R.

In addition, the presence of closed loops involving recirculated powder and the direct atomization of scrap provide environmental benefits by reducing the demand for feedstock derived from primary or secondary material production. Consistent with the allocation approach,

all environmental burdens associated with the production of input materials that generate pre-consumer scrap [36] are fully allocated to the upstream product systems responsible for scrap generation. Consequently, the downstream atomization process is exempt from accounting for these impacts. Overall, the equivalent carbon dioxide emissions associated solely with the consumption of incoming materials for the gas atomization of a given mass of powder within a predefined size range ($CO_{2\ mat}$) are obtained according to Eq. 7,

$$CO_{2\ mat} = \left[\sum_{j=1}^{m}\left(\frac{\alpha}{y_{fp}\cdot y_{pre}}\right)_j \cdot \left(CF_{raw} + CF_{pre}\right)_j\right] \cdot \frac{m_{pwd}}{y_{at}\cdot y_{sv}} \quad (7)$$

where, for each j-th feedstock material input:

- CF_{raw} is the carbon footprint of the raw material, computed in $kgCO_2/kg$ according to Eq. 6;
- CF_{pre} is the carbon footprint of the pre-processing phase, expressed in $kgCO_2$ per kg of material input.

2.3. Carbon footprint of powder production

In addition to the emissions associated with material inputs (computed in this study according to Eq. 7), process-related emissions resulting from the operation of powder production facilities have to be accounted for to provide a comprehensive cradle-to-gate assessment. These emissions include both direct and indirect contributions from melting and atomization, as well as auxiliary operations such as charge preparation, sieving, blending, and packing. The contribution of each unit process involved in powder production (within gate-to-gate system boundaries) is modeled using a black-box approach, in which all relevant sources of CO_2 emissions – such as electricity consumption, the use of inert gases, and other consumable resources – are quantified and normalized per unit mass of material input to the system. This modeling choice aligns with the structure of most Life Cycle Inventory (LCI) datasets, which typically report emissions and resource consumption per kilogram of material processed or treated at the input stage of the process. Moreover, using the mass of material entering each unit process as a reference also facilitates consistent integration of process yields, in line with the aim of this study, and provides a basis for propagating impacts across interconnected stages. In the context of powder production, where yield factors may be significantly lower than 1 (particularly during sieving), allocating impacts to the input avoids underestimation of emissions per unit of usable powder produced. Accordingly, the total process-related CO_2 emissions associated with powder manufacturing ($CO_{2\ mfg}$) are calculated using Eq. 8,

$$\begin{aligned} CO_{2\ mfg} &= \sum_{j=1}^{m}\left(\frac{m_{feed}}{y_{fp}}\cdot CF_{fp}\right)_j + \sum_{k=1}^{p}\left(\frac{m_{scr}}{y_{sp}}\cdot CF_{sp}\right)_k + m_{ch}\cdot CF_{ga} \\ &\quad + m_{at}\cdot CF_{sv} + m_{sv}\cdot CF_{pk} \\ &= \left[\sum_{j=1}^{m}\left(\frac{\alpha\cdot CF_{fp}}{y_{fp}\cdot y_{at}\cdot y_{sv}}\right)_j + \sum_{k=1}^{p}\left(\frac{\beta\cdot CF_{sp}}{y_{sp}\cdot y_{at}\cdot y_{sv}}\right)_k + \frac{CF_{ga}}{y_{at}\cdot y_{sv}} + \frac{CF_{sv}}{y_{sv}} + CF_{pk}\right]\cdot m_{pwd} \end{aligned} \quad (8)$$

where, in addition to the parameters previously defined and following the scheme in Fig. 1,

- CF_{fp} is the carbon footprint of the feedstock preparation process, expressed in $kgCO_2$ per kg of material input;
- CF_{sp} is the carbon footprint of the scrap preparation process, expressed in $kgCO_2$ per kg of material input;
- CF_{ga} is the carbon footprint of the gas atomization process, expressed in $kgCO_2$ per kg of material input;
- CF_{sv} is the carbon footprint of the sieving and blending process, expressed in $kgCO_2$ per kg of material input;
- CF_{pk} is the carbon footprint of the packing process, expressed in $kgCO_2$ per kg of material input.

In the formulation of Eq.8, the emissive contributions associated with charge preparation – such as cutting operations or any required cleaning or specific treatments – are considered separately for the mass of material sourced from primary/secondary feedstock and that originating from bulky scrap, due to the differing supply conditions that may necessitate distinct preparatory processes. Moreover, the specific emission factors associated with each unit process may vary significantly depending on plant configuration, equipment characteristics, resource suppliers, and the local energy mix. These factors are explicitly incorporated into the model to ensure an accurate representation of the overall environmental impact across different scenarios, as further detailed in Section 3.

3. Case study and data inventory

To clarify the applicability of the proposed model, AISI 316L powder production was selected as a case study. Three scenarios were analyzed: Scenario A (Section 3.1) represents an industrial production of AM powders and illustrates the use of the model with a heterogeneous feedstock charge. Scenario B (Section 3.2) explores the sensitivity of the carbon footprint to variations in charge composition. Scenario C (Section 3.3) accounts for variations in process yields by considering the industrial applicability of powders across the full particle size distribution (PSD) resulting from gas atomization. Table 1 provides a concise overview of the main objectives, feedstock compositions, sieving yields, particle size distributions, and key assumptions for each scenario. The data inventory combines primary data with secondary data from commercial databases and recent literature. Best- and worst-case assumptions are considered to reflect uncertainties in key parameters.

3.1. Scenario A: assessment of a prototypical industrial production

Scenario A represents a prototypical industrial production route for gas-atomized powders in the 20–63 μm range, intended for use in PBF-LB/M. The atomization feedstock consists of a heterogeneous charge comprising pre-alloyed AISI 316L bars, pure elemental metals, and an off-specification powder fraction originating from previous production cycles. The charge composition follows the proportions (α and γ) reported in Table 2, which are designed to ensure the targeted chemical composition of the resulting powder. This scenario does not consider the

Table 1
Overview of the three scenarios considered in the case study of AISI 316L powder production.

Scenario	A	B	C
Focus/ Objective	Prototypical industrial production	Sensitivity to charge composition	Sensitivity to PSD utilization
α (feedstock)	0.81 (pre-alloyed bars, pure metals)	Balance (pre-alloyed bars)	0.81 (as in Scenario A)
β (bulky scrap)	–	0.00–0.90	–
γ (recirculated powder)	0.19	0.10–0.50	0.19 (as in Scenario A)
Sieving yield (y_{sv})	0.38	0.38–0.45	0.80
PSD considered	20–63 μm	20–63 μm	1–120 μm
Main assumptions	Based on average industrial data; Scrap not included	Parametric variation to explore decarbonization potential	Considers full usable PSD; Impact redistributed accordingly

Table 2
Crucible charge composition and carbon footprint of material production and pre-manufacturing (Scenario A).

Crucible charge	Quantity (−)	CF_{raw} ($kgCO_2/kg$), Average [Range]	CF_{pre} ($kgCO_2/kg$), Average [Range]
Pre-alloyed AISI 316L (bar stock)	$\alpha_1 = 0.42$	5.57 [5.30–5.84]	0.45 [0.31–0.58]
Chromium (commercial purity, bar stock)	$\alpha_2 = 0.07$	20.70 [19.70–21.70]	0.76 [0.66–0.86]
Iron-Molybdenum alloy (bar stock)	$\alpha_3 = 0.02$	14.95 [14.20–15.70]	0.71 [0.51–0.91]
Iron (commercial purity, bar stock)	$\alpha_4 = 0.24$	1.58 [1.50–1.66]	0.29 [0.23–0.34]
Manganese (commercial purity, bar stock)	$\alpha_5 = 0.01$	3.66 [3.48–3.83]	0.47 [0.43–0.51]
Nickel (commercial purity, bar stock)	$\alpha_6 = 0.05$	7.57 [7.18–7.95]	0.21 [0.18–0.24]
Recirculated powder	$\gamma = 0.19$	Internal loop material	No pre-processing operations

inclusion of scrap as part of the charge (i.e., $\beta = 0$). The carbon footprint values for the input materials (CF_{raw} and CF_{pre}) are also listed in Table 2. These values were either directly retrieved or, when necessary, derived by allocating emissions to the input material flows, from the Granta Selector 2025 R1 database (version 25.1.2). The database provides life-cycle data consistent with industrial average production backgrounds for the relevant resource and material classes. For each input, the carbon footprint reflects the expected typical-grade production practices. For example, the CF_{raw} value for AISI 316L bars accounts for an average recycled content of 35 % in the actual material supply.

Gate-to-gate inventory data for energy and resource consumption were compiled based on 2023 operational averages provided by MIM-ETE S.r.l. for a powder production route employing closed-coupled gas atomization (CCA). The sources of environmental impact considered in the analysis are listed in Table 3 (detailed figures are omitted for confidentiality), together with the carbon footprint associated with each unit operation, expressed in $kgCO_2$ per kilogram of input material processed. Specifically, the GHG emission intensity of electricity was assumed to be 0.210 ± 10 % $kgCO_2/kWh$, based on the 2023 average for the EU27 region as reported by the European Environment Agency [37]. Carbon footprint values for nitrogen and argon were set at 0.17 ± 10 % $kgCO_2/Nm^3$ and 0.34 ± 10 % $kgCO_2/Nm^3$, respectively, based on primary data provided by the gas supplier. The carbon intensities of other consumables, such as refractory materials used during the CCA process (see also Ref. [24]) and the plastic containers used for final packaging, were sourced from the Granta Selector 2025 R1 database to ensure consistency throughout the analysis. The yield factors applied to the feedstock pre-processing, feedstock preparation, and gas atomization steps were assumed to be 0.95 (y_{pre}), 0.995 (y_{fp}), and 0.98 (y_{at}), respectively. For the sieving and blending stage, the proportion of powder with a granulometry within the specified particle size range relative to the total atomized powder mass was set at 0.38 (y_{sv}), based on industrial estimates.

Table 3
Estimated carbon footprint of the main unit processes in powder production.

Unit process	Accounted impact(s)	CF ($kgCO_2/kg$), Average [Range]
Feedstock preparation	Electrical energy	3.9 [3.5–4.3] × 10^{-3}
Gas atomization	Electrical energy; Nitrogen gas; Refractories	8.6 [7.8–9.4] × 10^{-1}
Sieving and blending	Electrical energy; Argon gas	4.6 [4.1–5.1] × 10^{-2}
Packing	Electrical energy; Plastic packaging (bottles); Argon gas; Silica bag	1.1 [1.0–1.2] × 10^{-1}

3.2. Scenario B: effects of variation in charge composition

Scenario B explores the environmental impact of modifying the atomization charge composition by varying the proportions of virgin materials, recycled or scrap inputs, and off-specification powders. According to the adopted modeling assumptions (i.e., the 100:0 allocation approach [33]), increasing the share of secondary raw materials and enhancing the recovery of waste are expected to significantly reduce the overall carbon footprint [25]. This scenario aims to quantify these potential benefits through the parametric model developed in the present study. As previously noted in the discussion of Eq. 3, the theoretical flexibility of the three normalized mass input parameters (α, β, and γ) to vary independently within the [0,1] range is constrained in practice by operational limitations. In particular, the use of recirculated powder poses technical challenges due to its high surface-area-to-volume ratio compared to bulk metals, which reduces the efficiency of induction melting. A common industrial practice is to first melt the bulk charge and subsequently introduce the powder once a liquid phase has been established. However, this approach typically results in longer process times and higher electricity consumption, and may increase the risk of oxidation. Literature reports powder recirculation rates in the range of 10–15 % [25], while values up to 40–50 % are considered technically feasible by industrial practitioners. On the other hand, the use of bulky scrap materials as a feedstock substitute in gas atomization may be constrained in industrial practice by regulatory and certification requirements. Nonetheless, laboratory-scale experiments have demonstrated the feasibility of incorporating scrap at levels of up to 100 % of the atomization charge mass [24,25], highlighting a promising direction for further investigation.

Based on these considerations, and while maintaining the mass balance constraints defined in Eq. 3 (i.e., $\alpha + \beta + \gamma = 1$), the ratio γ (representing the mass fraction of recirculated powder, m_{rec}, relative to the total charge mass, m_{ch}) was varied from 0.1 to 0.5. The ratio β (corresponding to the share of bulky scrap, m_{scr}, relative to m_{ch}) was varied from 0 to a maximum of 0.9. The remaining fraction α (i.e., the ratio of m_{feed} to m_{ch}) was computed as $\alpha = 1 - (\beta + \gamma)$. For α, it was assumed that the input consisted of pre-alloyed AISI 316L bar stock. The associated carbon footprint (CF_{raw}) was computed using Eq. 6, with values of 7.49 [7.12–7.85] $kgCO_2/kg$ for primary material production (i.e., CF_V) and 2.02 [1.92–2.12] $kgCO_2/kg$ for recycling (i.e., CF_R), based on data from the Granta Selector 2025 R1 database. The recycled content of the material supply, R, was parametrically varied from 0 % to 100 % in 25 %-increments.

The estimated carbon footprint values for the main unit processes involved in powder production were retained as reported in Table 3. While this assumption is unlikely to significantly affect the pre- or post-atomization stages, it may require validation for gas atomization, which is the main contributor to overall impacts. To explore this, industrial data were analyzed for correlations between energy/resource consumption and the ratio of powder to total feedstock mass. The analysis showed no clear trend, suggesting that factors such as batch timing or the thermal state of the furnace lining (e.g., preheating from previous runs) may have a greater influence. Therefore, the ±9 % variability assumed for gas atomization was considered representative of industrial conditions and sufficient to account for such fluctuations. The yield for bulky scrap preparation (y_{sp}) was conservatively set at 0.90 to account for material losses from surface cleaning, removal of oxidized/corroded/contaminated layers, and handling inefficiencies. Accordingly, a conservative carbon footprint of 0.2–0.3 $kgCO_2/kg$ of input material was assumed for scrap preparation, reflecting the additional energy demand of these mechanical operations. Furthermore, the impact of increasing the sieving yield (y_{sv}) from 38 % to 45 % was evaluated.

3.3. Scenario C: effects of variation in overall yield factor

Previous Scenarios A and B focused on powder production within a

defined particle size range (20–63 μm) for PBF-LB/M applications, assuming that the remaining fractions were off-specification and destined for closed-loop recycling within the powder production plant. Based on the equations proposed in Section 2, this assumption entails obvious modeling implications when referring to the unit mass of produced powder, since the process yield directly affects both the energy efficiency and the carbon footprint per kilogram of usable powder. Although referring to different materials, Martin et al. [18] already reported a specific energy consumption of 11.5 kWh/kg for aluminum powder production within a targeted AM particle size range, which can increase to over 50 kWh/kg when off-spec particles are discarded and typical yields below 20–40 % are considered (resulting in emissions higher than 25 $kgCO_2$/kg of AM powder). However, the broad applicability and compatibility of as-atomized AISI 316L stainless steel powders across various powder metallurgical (PM) processes support the efficient use of nearly the entire as-atomized particle size distribution (PSD), as confirmed by literature:

- *Fine powders* (< 20 μm) can be used for Metal Injection Molding (MIM) and Binder Jetting. These powders are effective in MIM and Micro-MIM, where particle sizes typically below 22 μm [38] enable the production of components with densities close to 99 %, ultimate tensile strengths of approximately 505 MPa, and elongations of around 50 % [39,40]. Although flowability issues may arise [41], these powders are also appropriate for Binder Jetting, allowing the fabrication of green parts with densities around 60 % and sintered components with densities exceeding 98 % [42,43].
- *Mid-sized powders* are widely employed across several PM technologies, including both AM-based processes [44,45] and coating deposition techniques such as High Velocity Oxygen Fuel (HVOF), Plasma Spraying (PS), and Cold Spraying (CS). Cold Spraying typically employs spherical AISI 316L powders sized between 5 and 45 μm, producing dense coatings with porosity below 1 %, suitable for corrosive environments [46]. Compared to PBF-LB/M, the average PSD in thermal spray applications tends to shift toward finer ranges, often within 20–70 μm [46–49], or may even include finer fractions [46,50]. Thermal spray techniques such as HVOF and plasma spraying commonly utilize PSDs in the 10–45 μm and 20–53 μm ranges, producing thick coatings with porosity below 0.5 % and good corrosion resistance [51–53].
- *Large powders* (> 63 μm, typically up to around 106 μm), are successfully employed in the deposition of AISI 316L coatings by Laser Cladding, resulting in robust metallurgical bonds with excellent wear and corrosion resistance [54–56]. Similarly, Directed Energy Deposition (DED) processes utilize powders in the 44–106 μm range, with very low variability in reported PSDs [57–59] compared to previously discussed AM processes. Electron Beam Melting (EBM) effectively employs powders sized below 106–150 μm, most commonly in the 45–105 μm [60,61] or 53–150 μm ranges [62–64]. Finally, Hot Isostatic Pressing (HIP) can profitably process powders covering a wide portion of the as-atomized PSD. Excluding fine powders, which can lead to oxide-based inclusions (e.g., PPBs), powders up to 250 μm have been successfully processed, achieving >99 % density and maintaining excellent mechanical properties [65].

Overall, as-atomized AISI 316L powders can be effectively employed across a broad particle size spectrum, depending on the specific requirements of the downstream processing route. This enables optimized resource utilization, reduces material losses, and implicitly increases the overall process yield. In Scenario C, the cradle-to-gate carbon footprint calculated in Scenario A was reallocated according to a representative post-atomization powder size distribution consisting of 3 % of particles below 20 μm, 38 % in the 20–63 μm range, 39 % between 63 and 120 μm, and 20 % above 120 μm (for internal recirculation), resulting in a net sieving yield (y_{sv}) of 0.80.

4. Results and discussion

Fig. 2 illustrates the carbon footprint results per kilogram of powder produced in the 20–63 μm particle size range, under the assumptions defined for Scenario A (Section 3.1). The error bar reflects the expected operational and input data uncertainties. The contributions from each powder production phase (computed according to Eq. 8) are shown separately from those associated with the input materials constituting the heterogeneous charge (Eq. 7). The total carbon footprint amounts to 17.4 ± 1.2 $kgCO_2$/kg powder, with the majority share (approximately 85 %) attributable to the input materials. Within this category, raw material production emerges as the primary source of emissions, with a carbon footprint at least one order of magnitude higher than that of pre-processing in most cases (cf. Table 2). The powder production phase, which is mainly driven by energy and resource consumption during gas atomization, accounts for 2.5 ± 0.2 $kgCO_2$/kg powder. These results are consistent with those reported by Ehmsen et al. [4], who quantified the cumulative energy demand and carbon footprint of nickel-free stainless steel (commercially branded Medidur) powders produced in the 10–53 μm range via CCA using nitrogen as the inert gas. Their GWP values ranged from 0.69 to 5.03 kg CO_2/kg powder, depending on the electricity mix and operational parameters considered. From a mitigation standpoint, besides reducing the environmental impact of the gas atomization process by increasing efficiency or switching to renewable energy sources, the results in Fig. 2 underscore the substantial influence of upstream material sourcing strategies. For example, using exclusively AISI 316L pre-alloyed bars (while keeping the recirculated powder fraction at $\gamma = 0.19$ and applying the impact values in Table 2) would result in a total carbon footprint of 16.4 ± 1.2 $kgCO_2$/kg powder. This observation provides the rationale for the subsequent discussion of Scenario B, wherein the implications of feedstock compositional changes on overall environmental performance are examined.

4.1. Effects of variations in charge composition

Fig. 3 presents the variation in the carbon footprint results for the production of 1 kg of powder in the 20–63 μm particle size range, as a function of the relative fractions of pre-alloyed bars, bulky scrap, and recirculated powder, all made of AISI 316L. The charge composition parameters γ (i.e., m_{rec}/m_{ch}, shown here at 10 %, 30 %, and 50 %), β (i.e., m_{scr}/m_{ch}, up to a maximum of 90 %), and α, calculated as the remainder to fulfill the mass balance condition $\alpha + \beta + \gamma = 1$, were varied parametrically based on the assumptions outlined in Section 3.2. For each

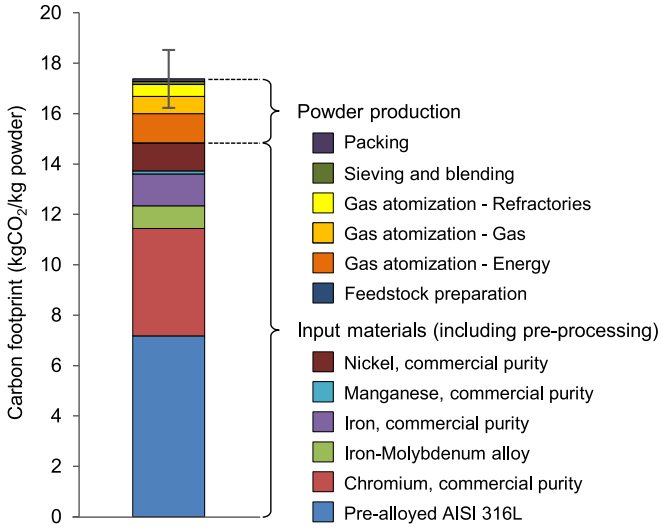


Fig. 2. Cradle-to-gate carbon footprint results for a prototypical industrial production (Scenario A).

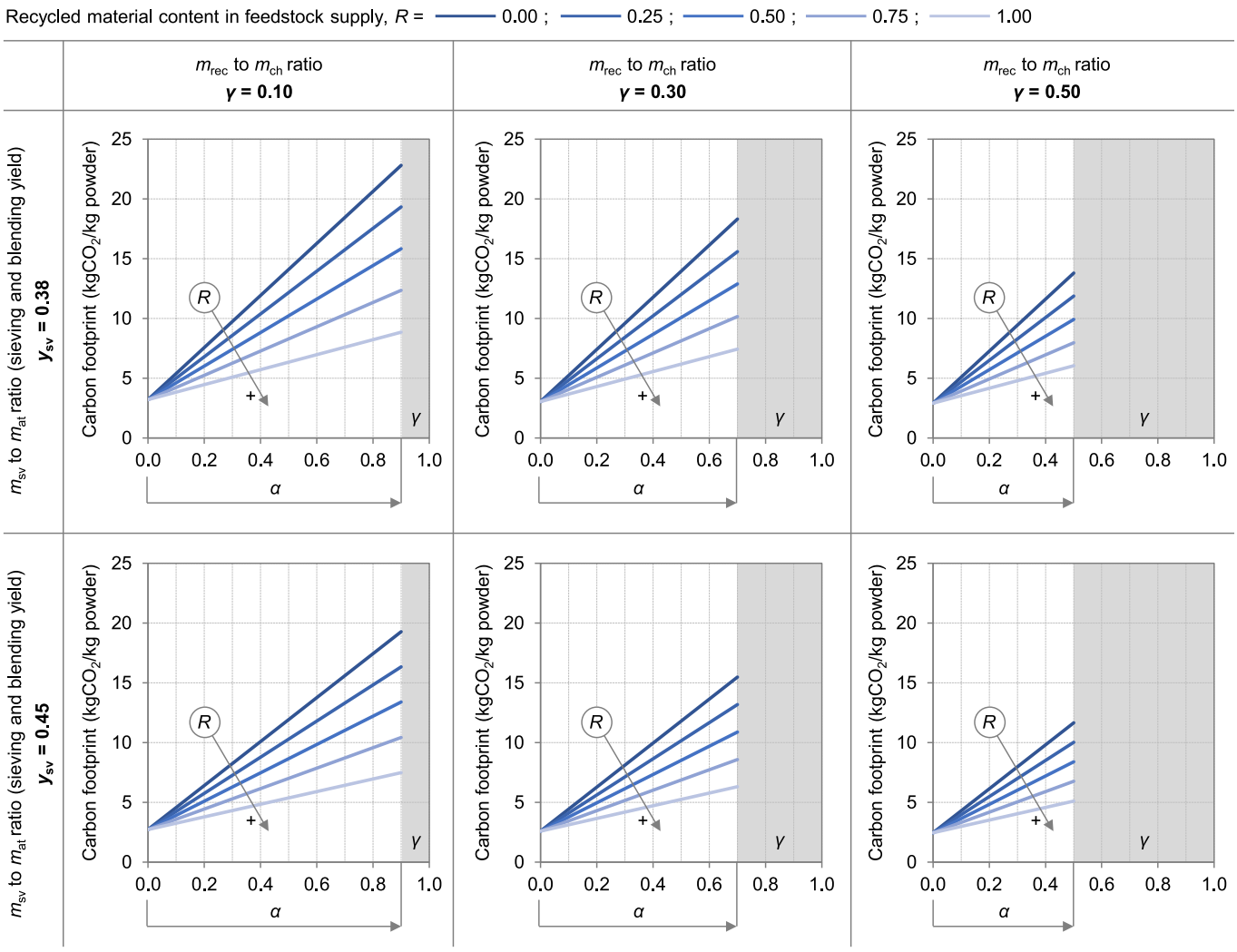


Fig. 3. Cradle-to-gate carbon footprint (average) results as a function of the material charge (Scenario B).

combination of these parameters, the results are plotted as a function of R, representing the recycled material content in the supply of pre-alloyed bars (cf. Eq. 6). The graphs in Fig. 3 illustrate a selected subset, deemed relevant for discussion, of the possible outcomes generated by the model described in Section 2, which enables the preliminary evaluation of any potential feedstock configuration introduced into the gas atomizer crucible.

The results highlight substantial, albeit expected, reductions in carbon footprint that can be achieved by increasing (*i*) the share of pre-consumer recycled content, (*ii*) the recycled content in the supply of pre-alloyed AISI 316L bars, and (*iii*) the overall process yield. Specifically, starting from a hypothetical reference configuration with a yield of 0.38 (as in Scenario A), composed entirely of virgin material for the pre-alloyed bars ($R = 0$) and incorporating 10 % recirculated powder (i.e., $\gamma = 0.1$, $\beta = 0$, and $\alpha = 0.9$), the carbon footprint is estimated at 22.8 ± 1.5 $kgCO_2$ per kg of powder. Several decarbonization pathways can be identified. Increasing the share of recirculated powder to $\gamma = 0.3$ would reduce the carbon footprint to 18.3 ± 1.2 $kgCO_2$/kg powder, corresponding to a reduction of approximately 20 %. Further increasing γ to 0.5 would lower the footprint to 13.8 ± 0.9 $kgCO_2$/kg powder (≈ 39 % reduction). Alternatively, maintaining the same charge composition ($\gamma = 0.1$, $\beta = 0$, $\alpha = 0.9$), increasing R to 50 % would decrease the footprint to 15.8 ± 1.2 $kgCO_2$/kg powder (≈ 31 % reduction), and increasing R to 100 % would further reduce it to 8.9 ± 0.8 $kgCO_2$/kg powder (≈ 61 % reduction). Or else, raising the yield from 0.38 to 0.45 would reduce the total required material input (m_{mat}, cf. Eq. 5) from 2.83 kg to 2.39 kg per kilogram of produced powder, resulting in a carbon footprint of 19.3 ± 1.3 $kgCO_2$/kg powder (≈ 15 % reduction).

According to the adopted modeling approach, the lowest impact values are achieved when the recycled and recirculated material content is maximized. In the cases where the combined share of γ and β equals one (and, consequently, $\alpha = 0$), the environmental burden associated with input materials is limited to the scrap preparation phase (Fig. 1), which is comparatively low relative to all other impact contributions. Under these conditions, the total carbon footprint would decrease to below 3.2 ± 0.4 $kgCO_2$/kg powder for $y_{sv} = 0.38$ and 2.7 ± 0.3 $kgCO_2$/kg powder for $y_{sv} = 0.45$. These results are consistent with other studies reported in the literature, even though they refer to different materials. Monti et al. [66] demonstrated the feasibility of producing high-quality Al-5Cu-3Ti-1Cr-1Fe powders for PBF-LB/M from a feedstock composed of 100 % recycled aluminum 2024, Ti-6Al-4V scrap, and AISI 316L scrap, achieving a ≈ 50 % reduction in carbon footprint (15.5 ± 1.0 $kgCO_2$/kg versus 31.5 ± 1.8 $kgCO_2$/kg for powders produced from virgin materials). Similarly, Benedetti et al. [25] reported that producing Inconel 718 powder feedstock from bulky scrap can lower both carbon footprint and energy demand by over 90 % relative to conventional production routes.

Although the technological feasibility of some configurations shown in Fig. 3 – particularly with regard to powder quality – is not assessed in this study (despite partial support from the literature reviewed in

Section 1.1) and remains outside its scope, the presented results are intended to highlight the potential extent of upstream decarbonization. Furthermore, the parametric model introduced in Section 2, together with the corresponding results, may serve as a decision-support tool. Once a target threshold for the maximum allowable carbon footprint is defined (e.g., 5.0 $kgCO_2$/kg powder), feasible charge compositions and process configurations that comply with this constraint can be readily identified. From a methodological standpoint, assuming equivalent powder performance ensures a consistent functional unit for the cradle-to-gate LCA. However, if powders produced from recycled materials or bulky scrap were to exhibit significantly different material properties or AM process performance (e.g., higher defect rates, altered mechanical behavior, or increased energy demand during printing), any environmental benefits gained from decarbonizing powder production could be offset by downstream penalties. In such a case, extending the LCA boundaries would be necessary to better contextualize the environmental implications of closed-loop material recycling in powder production.

4.2. Effects of variations in atomization process yield

In Scenario C, it is assumed that all atomized powder particles with diameters below 120 μm can be considered useful powder. This includes not only the typical particle size range of 20–63 μm used in PBF-L/M, but also finer particles below 20 μm (which may be suitable in Binder Jetting or Metal Injection Molding) and coarser particles in the 63–120 μm range (which may be employed for Directed Energy Deposition or other processes), as discussed in Section 3.3. Expanding the definition of usable powder, and thereby increasing the area under the particle size distribution (PSD) curve that contributes to m_{pwd}, leads to a higher sieving yield ($y_{sv} = 0.80$). If all other assumptions and impact factors are kept consistent with those used in Scenario A (as detailed in Section 3.1), the application of Eq. 7 and Eq. 8 yields a total carbon footprint of 8.3 ± 0.5 $kgCO_2$ per kg of powder within the extended range of 1–120 μm (hereafter referred to as $m_{pwd,1–120}$).

The mass breakdown of 1 kg of $m_{pwd,1–120}$ is (*i*) 0.04 kg of sub-20 μm powder ($m_{pwd,<20}$), (*ii*) 0.47 kg of 20–63 μm powder ($m_{pwd,20–63}$), and (*iii*) 0.49 kg of 63–120 μm powder ($m_{pwd,63–120}$). To allocate the impact to each individual powder fraction, while ensuring consistency with the result obtained for the batch of 1 kg of useful powder in the 1–120 μm range, Eq. 9 could be proposed,

$$CE_i = k_i \cdot CE_{1-120} \cdot \frac{m_{pwd,1-120}}{m_{pwd,i}} \quad (9)$$

where:

- CE_i is the carbon footprint in $kgCO_2$ per kg of powder for the *i*-th fraction;
- k_i is the dimensionless redistribution coefficient for the *i*-th fraction;
- $CE_{1\text{-}120}$ is the carbon footprint in $kgCO_2$ per kg of powder in the 1–120 μm range;
- $m_{pwd,i}$ is the mass of the *i*-th powder size fraction (in kg);
- $m_{pwd,1–120}$ is the total mass of useful powder in the 1–120 μm range (=1 kg).

Eq. 9 expresses the conservation of total impact through the allocation among sub-fractions, ensuring that the sum of partial contributions equals the total batch footprint (i.e., a co-product allocation among three outputs of a single process). The k_i coefficients (*i*) define how the environmental burden is distributed among size fractions and (*ii*) allow the exploration of alternative allocation criteria, under the condition that the redistribution coefficients collectively equal one. The k_i values are assumed equal (i.e., $k_i = 1/3$) in this work. This assumption implies no significant environmental differentiation among powder fractions in their contribution to the overall carbon footprint, as all fractions originate from the same atomization batch under identical process conditions, and no fraction-specific treatments are expected that would disproportionately increase environmental impact. Additionally, this approach assumes a supply-unconstrained system: downstream processes (such as Binder Jetting or DED) are assumed to have sufficiently high (or effectively infinite) demand to utilize the full quantity of each usable fraction without surplus or waste. Under these conditions, the resulting carbon footprints for each powder fraction in Scenario C are summarized in Table 4.

The values highlight that, under the assumption of equal redistribution coefficients, the allocated footprint per unit mass is inversely related to the relative abundance of each fraction within the 1–120 μm usable range. The <20 μm fraction, which accounts for only about 4 % of the usable powder mass, is assigned a carbon footprint over ten times higher than that of the other two fractions. This outcome reflects the mathematical structure of Eq. 9, where smaller mass fractions receive proportionally larger specific impact values when the total impact is redistributed equally. By contrast, the 20–63 μm and 63–120 μm fractions show relatively similar and lower values. The disaggregation of the batch-level footprint across PSD sub-fractions should be regarded as an allocation exercise, aimed at providing a mathematical representation of how environmental burdens scale with relative yield within a single production batch, rather than as a direct measurement of fraction-specific environmental impacts. The same modeling approach was applied by Gobber et al. [24] when analyzing the influence of inert-gas pressure on the gas atomization of UNS S32760 powders produced from waste materials. This approach proved effective in comparing carbon-footprint trends under different atomization conditions, as increasing the inert-gas pressure (or, equivalently, the gas-to-metal ratio) shifts the PSD toward finer fractions.

Alternative allocation criteria (such as mass-, economic-, or process-based approaches) could be adopted in other decision contexts. However, all would lead to consistent conclusions regarding the benefits of broader PSD utilization. The difference in carbon footprint per kilogram of usable powder between Scenario A and Scenario C is driven primarily by the sieving yield. Scenario A assumes $y_{sv} = 0.38$ (only the 20–63 μm fraction), resulting in an average footprint of 17.4 ± 1.2 $kgCO_2$/kg usable powder. Scenario C, with $y_{sv} = 0.80$ (all powder <120 μm), yields 8.3 ± 0.5 $kgCO_2$/kg usable powder. These differences reflect a more efficient utilization of the atomized material, and suggest additional paths for powder decarbonization.

5. Conclusions and outlook

Metal additive manufacturing technologies are increasingly adopted in advanced manufacturing systems due to their potential to enhance material utilization efficiency, enable the fabrication of complex geometries, and streamline production logistics. However, these benefits are often counterbalanced by the high specific energy demands of the manufacturing stage and by the significant environmental burden associated with feedstock production, which remains a central contributor to the overall life cycle impacts of AM-ed components. This study introduced a parametric modeling framework for the cradle-to-gate carbon footprint assessment of metal powders produced via gas atomization. The methodology relies on a system of mass and carbon balance equations, allowing for the quantification of environmental impacts as a function of input material composition and powder size distribution.

Table 4
Hypothesis of carbon footprint allocation per powder fraction (Scenario C).

Powder fraction	$m_{pwd,i}/m_{at}$	$m_{pwd,i}/m_{pwd,1–120}$	CE_i ($kgCO_2$/kg powder)
< 20 μm	0.03	0.04	69.2 ± 4.2
20–63 μm	0.38	0.47	5.9 ± 0.4
63–120 μm	0.39	0.49	5.6 ± 0.3
> 120 μm	0.20	–	–

The framework enables the systematic analysis of feedstock variability, with a particular focus on heterogeneous charge configurations (including pre-alloyed bars or pure metals, bulky scrap, and recycled powder fractions).

Focusing on AISI 316L powder production, numerical analyses demonstrated that raw material inputs constitute the predominant source of carbon emissions in a prototypical industrial scenario, accounting for approximately 85 % of the total cradle-to-gate footprint. Increasing the proportion of pre-consumer recycled inputs or recirculated powder fractions, as well as maximizing the recycled content within pre-alloyed materials can result in substantial reductions in greenhouse gas emissions. Furthermore, expanding the acceptable range of powder size fractions enhances atomization yield, thereby lowering the specific carbon footprint per unit of usable powder. These findings are consistent with the anticipated benefits associated with circular economy practices and process efficiency improvements. However, while increasing recycled contents and improving atomization yield are recognized strategies for reducing environmental impacts, to the best of the authors' knowledge, no available studies provide a structured, quantitative, and comparative analysis that systematically examines the combined effects of heterogeneous feedstock compositions and powder size distributions on the cradle-to-gate carbon footprint of gas-atomized metal powders. Such an approach could establish the basis for developing a robust decision-support tool for process planning in gas atomization, with implications for industrial-scale powder production.

This study acknowledges some limitations. First, the results are specific to the case study analyzed, the modeling assumptions adopted, and the data inventory employed. The analysis follows the 100:0 approach, a cut-off methodology whereby pre-consumer recycled inputs enter the system with no upstream environmental burden; only the impacts associated with sorting, cleaning, and reprocessing (if any) are considered. Similarly, for materials with 100 % recycled content, only the impacts related to remelting and subsequent processing are included [36]. Whenever possible, primary data were used in accordance with LCA best practices. Nonetheless, the needed reliance on secondary data sources introduces uncertainties related to data quality, geographic variability in energy mixes, and differences in raw material production technologies. Should alternative datasets or allocation methods be used, the resulting carbon footprint values could vary significantly. Moreover, the parametric and deterministic modeling approach, although suitable for evaluating alternative scenarios and identifying viable decarbonization strategies, does not account for the temporal distribution of material flows, which would introduce stochastic effects beyond the intrinsic data uncertainty already considered in this study.

The assumption of equivalent powder performance across different feedstock compositions is necessary for the environmental comparison to be scientifically sound. While this assumption is supported by existing literature, it has not been experimentally validated within the scope of this study and should be verified on a case-by-case basis. Additionally, the framework assumes supply-unconstrained conditions and does not account for potential logistical, economic, legal or technical barriers that may hinder the implementation of closed-loop recycling or the use of broader powder size distributions.

Lastly, gas atomization was treated in this study as a stand-alone process, whose resulting powders constitute a product per se, analogous to semi-finished products in steelmaking. Extending the analysis to downstream manufacturing routes such as AM and MIM would require defining a specific case study and integrating additional process-specific inventories (as shown by Monti et al. [66]). Reported specific electrical energy demands for metal PBF processes vary widely (commonly between 50 and 600 MJ/kg, according to Kellens et al. [67]), depending on machine type, processing parameters, and utilization rate [68,69]. In contrast, the energy required for the MIM forming step is typically lower, although debinding and sintering can substantially increase total energy use [70]. Owing to the variability of these figures and to the dependence of carbon footprints on local energy mixes, expanding the system boundaries would allow for a more rigorous cross-technology assessment. This remains a promising direction for future research, as the impacts of powder production may be offset by those arising during manufacturing or over the full product life cycle.

CRediT authorship contribution statement

Paolo C. Priarone: Writing – review & editing, Writing – original draft, Visualization, Methodology, Investigation, Formal analysis, Conceptualization, Validation. **Federico Simone Gobber:** Writing – review & editing, Writing – original draft, Investigation, Conceptualization, Validation. **Stefania Cacace:** Writing – review & editing, Writing – original draft, Resources, Investigation, Conceptualization, Validation.

Declaration of competing interest

The authors declare that they have no known competing financial interests or personal relationships that could have appeared to influence the work reported in this paper.

Acknowledgements

The authors gratefully acknowledge MIMETE S.r.l. for its support in the development of this study. In particular, they wish to thank Francesca Bonfanti and Maria Guzzoni (listed in alphabetical order) for providing primary data and for their insightful contributions to the definition of scenarios of industrial relevance.

Data availability

Additional data may be available from the authors upon reasonable request and with permission from MIMETE S.r.l.

References

[1] International Energy Agency (IEA), Greenhouse Gas Emissions from Energy Data Explorer, Available at: https://www.iea.org/data-and-statistics/data-tools/greenhouse-gas-emissions-from-energy-data-explorer. Lastly accessed November 2025.
[2] World Resources Institute (WRI), World Greenhouse Gas Emissions by Sector 2021 (Sankey flow chart), Available at, https://www.wri.org/data/world-greenhouse-gas-emissions-2021, 2025. Lastly accessed November 2025.
[3] M. Crippa, et al., GHG Emissions of all World Countries – JRC Science for Policy Report, 2025, Publications Office of the European Union, Luxembourg, 2025, https://doi.org/10.2760/9816914.
[4] S. Ehmsen, J. Conrads, M. Klar, J.C. Aurich, Environmental impact of powder production for additive manufacturing: carbon footprint and cumulative energy demand of gas atomization, J. Manuf. Syst. 82 (2025) 13–25, https://doi.org/10.1016/j.jmsy.2025.05.004.
[5] P.C. Priarone, A.R. Catalano, L. Settineri, Additive manufacturing for the automotive industry: on the life-cycle environmental implications of material substitution and lightweighting through re-design, Prog. Addit. Manuf. 8 (6) (2023) 1229–1240, https://doi.org/10.1007/s40964-023-00395-x.
[6] V. Madhavadas, D. Srivastava, U. Chadha, S.A. Raj, M.T. Sultan, F.S. Shahar, A. U. Shah, A review on metal additive manufacturing for intricately shaped aerospace components, CIRP J. Manuf. Sci. Technol. 39 (2022) 18–36, https://doi.org/10.1016/j.cirpj.2022.07.005.
[7] S. Ramadugu, S.R. Ledella, J.N. Gaduturi, R.R. Pinninti, V. Sriram, K.K. Saxena, Environmental life cycle assessment of an automobile component fabricated by additive and conventional manufacturing, Int. J. Interact. Des. Manuf. 18 (2024) 847–858, https://doi.org/10.1007/s12008-023-01532-0.
[8] S. Cecchel, Materials and technologies for lightweighting of structural parts for automotive applications, SAE Int J Mater Manuf 14 (1) (2021) 81–98. https://www.jstor.org/stable/27033986.
[9] M. Sireesha, J. Lee, A.S. Kiran, V.J. Babu, B.B. Kee, S. Ramakrishna, A review on additive manufacturing and its way into the oil and gas industry, RSC Adv. 8 (40) (2018) 22460–22468, https://doi.org/10.1039/C8RA03194K.
[10] T. Peng, Y. Wang, Y. Zhu, Y. Yang, Y. Yang, R. Tang, Life cycle assessment of selective-laser-melting-produced hydraulic valve body with integrated design and manufacturing optimization: a cradle-to-gate study, Addit. Manuf. 36 (2020) 101530, https://doi.org/10.1016/j.addma.2020.101530.
[11] R. Rahmani, B. Bashiri, S.I. Lopes, A. Hussain, H.S. Maurya, R. Vilu, Sustainable additive manufacturing: an overview on life cycle impacts and cost efficiency of laser powder bed fusion, J Manuf Mater Process 9 (1) (2025) 18, https://doi.org/10.3390/jmmp9010018.

[12] C. Spreafico, Prospective life cycle assessment of titanium powder atomization, J. Clean. Prod. 468 (2024) 143104, https://doi.org/10.1016/j.jclepro.2024.143104.
[13] C. Schade, Introduction to Metal Powder Production and Characterization, in: P. Samal, J. Newkirk (Eds.), ASM Handbook: Powder Metallurgy, ASM International, 2015, pp. 55–57, https://doi.org/10.31399/asm.hb.v07.a0006086.
[14] L.E.T. Mathias, V.E. Pinotti, B.F. Batistão, N. Rojas-Arias, G. Figueira, A. F. Andreoli, P. Gargarella, Metal powder as feedstock for laser-based additive manufacturing: from production to powder modification, J. Mater. Res. 39 (2024) 19–47, https://doi.org/10.1557/s43578-023-01271-8.
[15] J.J. Dunkley, Metal powder atomisation methods for modern manufacturing, Johnson Matthey Technol Rev 63 (2019) 226–232, https://doi.org/10.1595/205651319X15583434137356.
[16] T. Fedina, J. Sundqvist, J. Powell, A.F.H. Kaplan, A comparative study of water and gas atomized low alloy steel powders for additive manufacturing, Addit. Manuf. 36 (2020) 101675, https://doi.org/10.1016/j.addma.2020.101675.
[17] S. Zhang, K. Guo, Y. Qing, C. Liu, Research Progress on the preparation Technology of Spherical Alloy Powders for laser additive manufacturing, Materials 18 (14) (2025) 3385, https://doi.org/10.3390/ma18143385.
[18] J.H. Martin, J.E. Barnes, K.A. Rogers, J. Hundley, D.L. LaPlant, S. Ghanbari, J.-T. Tsai, D.F. Bahr, Additive manufacturing of a high-performance aluminum alloy from cold mechanically derived non-spherical powder, Commun. Mater. 4 (2023) 39, https://doi.org/10.1038/s43246-023-00365-4.
[19] S. Dhiman, R.S. Joshi, S. Singh, S.S. Gill, H. Singh, R. Kumar, V. Kumar, A framework for effective and clean conversion of machining waste into metal powder feedstock for additive manufacturing, Clean Eng Technol 4 (2021) 100151, https://doi.org/10.1016/j.clet.2021.100151.
[20] S. Dhiman, R.S. Joshi, S. Singh, S.S. Gill, H. Singh, R. Kumar, V. Kumar, Recycling of Ti6Al4V machining swarf into additive manufacturing feedstock powder to realise sustainable recycling goals, J. Clean. Prod. 348 (2022) 131342, https://doi.org/10.1016/j.jclepro.2022.131342.
[21] M. Gökelma, D. Celik, O. Tazegul, H. Cimenoglu, B. Friedrich, Characteristics of Ti6AL4V powders recycled from turnings via the HDH technique, Metals 8 (5) (2018) 336, https://doi.org/10.3390/met8050336.
[22] S. Cacace, V. Furlan, R. Sorci, Q. Semeraro, M. Boccadoro, Using recycled material to produce gas-atomized metal powders for additive manufacturing processes, J. Clean. Prod. 268 (2020) 122218, https://doi.org/10.1016/j.jclepro.2020.122218.
[23] V. Tebaldo, G. Gautier di Confiengo, D. Duraccio, M.G. Faga, Sustainable recovery of titanium alloy: from waste to feedstock for additive manufacturing, Sustainability 16 (1) (2024) 330, https://doi.org/10.3390/su16010330.
[24] F.S. Gobber, P.C. Priarone, A. Pennacchio, M.A. Grande, Effect of inert gas pressure on the properties and carbon footprint of UNS S32760 powders made from waste materials by gas atomization, J. Mater. Res. Technol. 33 (2024) 8814–8828, https://doi.org/10.1016/j.jmrt.2024.11.195.
[25] M. Benedetti, M. Perini, M. Vanazzi, A. Giorgini, G. Macoretta, C. Menapace, Atomized scrap powder feedstock for sustainable Inconel 718 additive manufacturing via LPBF: a study of static and fatigue properties, Prog. Addit. Manuf. 9 (2024) 1843–1856, https://doi.org/10.1007/s40964-023-00547-z.
[26] J. Richter, T. Wegener, R. Kratzsch, M. Vollmer, U. Peuker, T. Niendorf, On the structural integrity and fatigue performance of additively manufactured Ti-6Al-4V parts processed using mechanically recycled powders, Int. J. Fatigue 176 (2023) 107903, https://doi.org/10.1016/j.ijfatigue.2023.107903.
[27] M. Singh, S. Dhiman, H. Singh, R.A. Rahman Rashid, S. Palanisamy, Sustainable production of powder feedstock from machining waste using modulation-assisted drilling, Int. J. Adv. Manuf. Technol. 133 (2024) 5643–5655, https://doi.org/10.1007/s00170-024-14089-3.
[28] H.R. Bai, H.R. Zhang, J.F. Weng, B. Kong, H. Zhang, Purification behaviour of GH4169 scraps under argon atmosphere during vacuum induction melting, Mater. Res. Innov. 18 (2014), https://doi.org/10.1179/1432891714Z. 000000000702. S4-357-S4-362.
[29] L. Brabie, S. Kazi, A. Strondl, P. Mellin, T. Fedina, L. Leach, E. Hryha, Recycling Of 316 L Powder And Scrap From Additive Manufacturing Processing, in: Euro PM2024 Proceedings, EPMA, 2024, https://doi.org/10.59499/EP246277177.
[30] ISO 14040:2006, Environmental management - Life cycle assessment - Principles and framework. Published, Edition 2, 2006.
[31] ISO 14044:2006, Environmental management - Life cycle assessment - Requirements and guidelines. Published, Edition 1, 2006.
[32] European Commission - Joint Research Centre - Institute for Environment and Sustainability, International Reference Life Cycle Data System (ILCD) Handbook - General guide for Life Cycle Assessment - Detailed guidance. First edition March 2010. EUR 24708 EN, Publications Office of the European Union, Luxembourg, 2010.
[33] ISO 14067:2018, Greenhouse gases - Carbon footprint of products - Requirements and guidelines for quantification. Published, Edition 1, 2018.
[34] G. Hammond, C. Jones, Embodied Carbon - The Inventory of Carbon and Energy (ICE), Annex B: How to Account for Recycling. ©BSRIA BG 10/2011, 2011. ISBN 978 0 86022 703 8.
[35] M.F. Ashby, Materials and the environment: eco-informed material choice, Third Edition. Butterworth Heinemann/ Elsevier (2021), https://doi.org/10.1016/C2016-0-04008-1.
[36] L. Zampori, R. Pant, Suggestions for updating the product environmental footprint (PEF) method, JRC Technical Reports - European Commission (2019), https://doi.org/10.2760/424613.
[37] European Environment Agency (EEA), Greenhouse gas emission intensity of electricity generation, country level, Available at: https://www.eea.europa.eu/en/analysis/indicators/greenhouse-gas-emission-intensity-of-1/greenhouse-gas-emission-intensity-of-electricity-generation-country-level, 2025. Published 25 Oct 2024, Modified 27 Jun 2025, Lastly accessed July 2025.
[38] M. Aslam, F. Ahmad, P.S.M.B.M. Yusoff, K. Altaf, M.A. Omar, R.M. German, Powder injection molding of biocompatible stainless steel biodevices, Powder Technol. 295 (2016) 84–95, https://doi.org/10.1016/j.powtec.2016.03.039.
[39] A. Manonukul, S. Songkuea, P. Moonchaleanporn, M. Tange, Effect of weld line positions on the tensile deformation of two-component metal injection moulding, Int. J. Miner. Metall. Mater. 24 (2017) 1384–1393, https://doi.org/10.1007/s12613-017-1531-1.
[40] B. Hausnerova, M. Novak, Environmentally efficient 316L stainless steel feedstocks for powder injection Molding, Polymers 12 (6) (2020) 1296, https://doi.org/10.3390/polym12061296.
[41] S. Mirzababaei, S. Pasebani, A review on binder jet additive manufacturing of 316L stainless steel, J Manuf Mater Process 3 (3) (2019) 82, https://doi.org/10.3390/jmmp3030082.
[42] Y. Mao, J. Li, W. Li, D. Cai, Q. Wei, Binder jetting additive manufacturing of 316L stainless-steel green parts with high strength and low binder content: binder preparation and process optimization, J. Mater. Process. Technol. 291 (2021) 117020, https://doi.org/10.1016/j.jmatprotec.2020.117020.
[43] N. Lecis, M. Mariani, R. Beltrami, L. Emanuelli, R. Casati, M. Vedani, A. Molinari, Effects of process parameters, debinding and sintering on the microstructure of 316L stainless steel produced by binder jetting, Mater. Sci. Eng. A 828 (2021) 142108, https://doi.org/10.1016/j.msea.2021.142108.
[44] S. Ziri, A. Hor, C. Mabru, Combined effect of powder properties and process parameters on the density of 316L stainless steel obtained by laser powder bed fusion, Int. J. Adv. Manuf. Technol. 120 (2022) 6187–6204, https://doi.org/10.1007/s00170-022-09160-w.
[45] G. Huang, K. Wei, J. Deng, M. Liu, X. Zeng, High-power laser powder bed fusion of 316L stainless steel: defects, microstructure, and mechanical properties, J. Manuf. Process. 83 (2022) 235–245, https://doi.org/10.1016/j.jmapro.2022.08.066.
[46] A. Sova, S. Grigoriev, A. Okunkova, I. Smurov, Cold spray deposition of 316L stainless steel coatings on aluminium surface with following laser post-treatment, Surf. Coat. Technol. 235 (2013) 283–289, https://doi.org/10.1016/j.surfcoat.2013.07.052.
[47] L.H. Brassart, J. Besson, F. Delloro, D. Haboussa, F. Delabrouille, G. Rolland, Y. Shen, A.F. Gourgues-Lorenzon, Effect of various heat treatments on the microstructure of 316L austenitic stainless steel coatings obtained by cold spray, J. Therm. Spray Technol. 31 (2022) 1725–1746, https://doi.org/10.1007/s11666-022-01402-3.
[48] D. Kotoban, S. Grigoriev, A. Okunkova, A. Sova, Influence of a shape of single track on deposition efficiency of 316L stainless steel powder in cold spray, Surf. Coat. Technol. 309 (2017) 951–958, https://doi.org/10.1016/j.surfcoat.2016.10.052.
[49] R.F. Vaz, A. Silvello, J. Sanchez, V. Albaladejo, Cano I. García, The influence of the powder characteristics on 316L stainless steel coatings sprayed by cold gas spray, Coatings 11 (2) (2021) 168, https://doi.org/10.3390/coatings11020168.
[50] S. Adachi, N. Ueda, Effect of cold-spray conditions using a nitrogen propellant gas on AISI 316L stainless steel-coating microstructures, Coatings 7 (7) (2017) 87, https://doi.org/10.3390/coatings7070087.
[51] S. Adachi, N. Ueda, Surface hardness improvement of plasma-sprayed AISI 316L stainless steel coating by low-temperature plasma carburizing, Adv. Powder Technol. 24 (2013) 818–823, https://doi.org/10.1016/j.apt.2012.12.011.
[52] K. Palanisamy, S. Gangolu, Antony J. Mangalam, Effects of HVOF spray parameters on porosity and hardness of 316L SS coated Mg AZ80 alloy, Surf. Coat. Technol. 448 (2022) 128898, https://doi.org/10.1016/j.surfcoat.2022.128898.
[53] L. Zhao, E. Lugscheider, Influence of the spraying processes on the properties of 316L stainless steel coatings, Surf. Coat. Technol. 162 (1) (2003) 6–10, https://doi.org/10.1016/S0257-8972(02)00560-1.
[54] V. Pejaković, L.-M. Berger, S. Thiele, H. Rojacz, Ripoll M. Rodríguez, Fine grained titanium carbonitride reinforcements for laser deposition processes of 316L boost tribocorrosion resistance in marine environments, Mater. Des. 207 (2021) 109847, https://doi.org/10.1016/j.matdes.2021.109847.
[55] Z. Liu, C. Han, X. Cao, J. Guo, H. Li, Y. Lin, J. Yang, W. Liu, Microstructure and wear behavior of AISI 316L austenitic stainless steel coating fabricated by laser cladding and plasma nitriding, Mater. Lett. 383 (2025) 137951, https://doi.org/10.1016/j.matlet.2024. 137951.
[56] H. Ding, T. Yang, W. Wang, Y. Zhu, Q. Lin, J. Guo, Q. Xiao, L. Gan, Q. Liu, Optimization and wear behaviors of 316L stainless steel laser cladding on rail material, Wear 523 (2023) 204830, https://doi.org/10.1016/j.wear.2023.204830.
[57] A. Aversa, G. Marchese, E. Bassini, Directed energy deposition of AISI 316L stainless steel powder: effect of process parameters, Metals 11 (6) (2021) 932, https://doi.org/10.3390/met11060932.
[58] H. Balhara, B. Botcha, S.J. Wolff, S.T.S. Bukkapatnam, Ripple formations determine the heterogeneous microstructure of directed energy deposition (DED)-printed 316L components, Mater. Des. 227 (2023) 111756, https://doi.org/10.1016/j.matdes.2023.111756.
[59] H. Balhara, C. Yelkarasi, A. Erdemir, S.T.S. Bukkapatnam, Spatial characteristics of ultra hard coating on directed energy deposition (DED)-printed 316L with a novel ultra-fast boriding, J. Manuf. Process. 121 (2024) 92–99, https://doi.org/10.1016/j.jmapro.2024.04.094.
[60] G.G. Goviazin, D. Braun, E. Tiferet, S. Samuha, S. Hayun, A. Shirizly, D. Rittel, The effect of hot isostatic pressing on the thermomechanical behavior of electron beam powder-bed fusion SS316L, Prog. Addit. Manuf. (2025), https://doi.org/10.1007/s40964-025-01006-7.
[61] P. Tarafder, J. Xu, A. Wiberg, J. Moverare, Assessing the effect of scan strategies on the structure-property relationship in electron beam powder bed fusion processed

316L stainless steel, Mater. Des. (2025) 113837, https://doi.org/10.1016/j.matdes.2025.113837.
[62] Y. Zhong, L.E. Rännar, L. Liu, A. Koptyug, S. Wikman, J. Olsen, D. Cui, Z. Shen, Additive manufacturing of 316L stainless steel by electron beam melting for nuclear fusion applications, J. Nucl. Mater. 486 (2017) 234–245, https://doi.org/10.1016/j.jnucmat. 2016.12.042.
[63] L.E. Rännar, A. Koptyug, J. Olsén, K. Saeidi, Z. Shen, Hierarchical structures of stainless steel 316L manufactured by Electron beam melting, Addit. Manuf. 17 (2017) 106–112, https://doi.org/10.1016/j.addma.2017.07.003.
[64] S. Roos, C. Botero, J. Danvind, A. Koptioug, L.E. Rännar, Macro- and micromechanical behavior of 316LN lattice structures manufactured by Electron beam melting, J. Mater. Eng. Perform. 28 (2019) 7290–7301, https://doi.org/10.1007/s11665-019-04484-3.
[65] S. Irukuvarghula, H. Hassanin, C. Cayron, M. Aristizabal, M.M. Attallah, M. Preuss, Effect of powder characteristics and oxygen content on modifications to the microstructural topology during hot isostatic pressing of an austenitic steel, Acta Mater. 172 (2019) 6–17, https://doi.org/10.1016/j.actamat.2019.03.038.
[66] C. Monti, F.S. Gobber, M. Turani, K. Papis, P.C. Priarone, M. Actis Grande, M. Bambach, Evaluating the use of scrap metal to produce Al-5Cu-3Ti-1Cr-1Fe alloy powder for laser powder bed fusion, Sustain. Mater. Technol. 45 (2025) e01606, https://doi.org/10.1016/j.susmat.2025.e01606.
[67] K. Kellens, M. Baumers, T.G. Gutowski, W. Flanagan, R. Lifset, J.R. Duflou, Environmental dimensions of additive manufacturing: mapping application domains and their environmental implications, J. Ind. Ecol. 21 (S1) (2017) S49–S68, https://doi.org/10.1111/jiec.12629.
[68] S. Kokare, J.P. Oliveira, R. Godina, Life cycle assessment of additive manufacturing processes: a review, J. Manuf. Syst. 68 (2023) 536–559, https://doi.org/10.1016/j.jmsy.2023.05.007.
[69] M. Taghian, M.H. Mosallanejad, E. Lannunziata, G. Del Greco, L. Iuliano, A. Saboori, Laser powder bed fusion of metallic components: latest progress in productivity, quality, and cost perspectives, J. Mater. Res. Technol. 27 (2023) 6484–6500, https://doi.org/10.1016/j.jmrt.2023.11.049.
[70] S.B. Hein, Petzodt., Evaluating metal injection Molding as a green production technology. PIM, International 17 (2) (2023) 61–69 (ISSN 2050-9707 (Online edition), Inovar Communications Ltd).